Research Square

Preprints are preliminary reports that have not undergone peer review.
They should not be considered conclusive, used to inform clinical practice,
or referenced by the media as validated information.

Clinical and Imaging Findings for the Evaluation of Large Rathke's Cleft Cysts and Cystic Craniopharyngiomas

Chung-Han Yang
Taipei Veterans General Hospital
Chia-Hung Wu
Taipei Veterans General Hospital
Te-Ming Lin
Taipei Veterans General Hospital
Shu-Ting Chen
Taipei Veterans General Hospital
Wei-An Tai
Taipei Veterans General Hospital
Kai-Wei Yu
Taipei Veterans General Hospital
Chao-Bao Luo
Taipei Veterans General Hospital
Jiing-Feng Lirng
Taipei Veterans General Hospital
Feng-Chi Chang (fcchang374@gmail.com)
Taipei Veterans General Hospital

Research Article

Keywords: Rathke's cleft cyst, craniopharyngioma, sellar mass, magnetic resonance imaging

Posted Date: March 13th, 2023

DOI: https://doi.org/10.21203/rs.3.rs-2664087/v1

License: This work is licensed under a Creative Commons Attribution 4.0 International License.
Read Full License

Additional Declarations: No competing interests reported.

Version of Record: A version of this preprint was published at Pituitary on May 25th, 2023. See the published version at https://doi.org/10.1007/s11102-023-01326-3.

Abstract

Purpose

Large Rathke's cleft cysts (LRCCs) and cystic craniopharyngiomas (CCPs) arise from the same embryological origin and may have similar MR presentations. However, the two tumors have different management strategies and outcomes. This study was designed to evaluate the clinical and imaging findings of LRCCs and CCPs, aiming to evaluate their pretreatment diagnosis and outcomes.

Methods

We retrospectively enrolled 20 patients with LRCCs and 25 patients with CCPs. Both tumors had a maximal diameter of more than 20 mm. We evaluated the patients' clinical and MR imaging findings, including symptoms, management strategies, outcomes, anatomic growth patterns and signal changes.

Results

The age of onset for LRCCs versus CCPs was 49.0 ± 16.8 versus 34.2 ± 22.2 years ($p = .022$); the following outcomes were observed for LRCCs versus CCPs: 1) postoperative diabetes insipidus: 6/20 (30%) versus 17/25 (68%) ($p = .006$); and 2) posttreatment recurrence: 2/20 (10%) versus 10/25 (40%) ($p = .025$). The following MR findings were observed for LRCCs versus CCPs: 1) solid component: 7/20 (35%) versus 21/25 (84%) ($p = .001$); 2) thick cyst wall: 2/20 (10%) versus 12/25 (48%) ($p = .009$); 3) intracystic septation: 1/20 (5%) versus 8/25 (32%) ($p = .030$); 4) snowman shape: 18/20 (90%) versus 1/25 (4%) ($p < .001$); 5) off-midline extension: 0/0 (0%) versus 10/25 (40%) ($p = .001$); and 6) oblique angle of the sagittal long axis of the tumor: 89.9° versus 107.1° ($p = .001$).

Conclusions

LRCCs can be differentiated from CCPs based on their clinical and imaging findings, especially their specific anatomical growth patterns. We suggest using the pretreatment diagnosis to select the appropriate surgical approach and thus improve the clinical outcome.

Introduction

Rathke's cleft cysts (RCCs) and cystic craniopharyngiomas (CCPs) are common cystic lesions of the sellar-suprasellar region. After Rathke's pouch forms between the anterior and intermediate pituitary gland, the residual Rathke's cleft normally closes in humans. The cells lining Rathke's cleft are thought to be the origin of various lesions, including RCCs and craniopharyngiomas [1, 2]. RCCs are typically small, asymptomatic, pure cystic lesions lying in the pars intermedia between the anterior and posterior pituitary lobes [2, 3]. Tumor sizes greater than 20 mm (considered large RCCs [LRCCs]) are rare and usually

present as a sellar lesion with suprasellar extension[4, 5]. LRCCs can be symptomatic from compression of its adjacent structures [2]. Craniopharyngiomas have been hypothesized to arise from embryonic squamous cell rests of an incompletely involuted craniopharyngeal duct or Rathke's pouch, which is considered a common ectodermal origin as in LRCC [6, 7]. Craniopharyngiomas are classified into two different histological subtypes: adamantinomatous and papillary. The tumor composition can also be classified as either solid or cystic; if the cystic component represents > 50% of the lesion volume, the tumor should be defined as cystic [8]. Approximately 90% of adamantinomatous craniopharyngiomas are predominantly cystic [9]. Patients with CCPs tend to have clinical symptoms and need further treatment.

The differential diagnosis of RCC and CCP is usually not difficult and is based on their clinical presentations, tumor size, and tumor location. When both cystic tumors reach considerable sizes, the clinical differential diagnosis may sometimes be challenging because the two tumors can share similar clinical presentations, such as headache, visual impairment, and endocrine dysfunction [10, 11]. Their imaging differentiation is especially difficult when the CCP presents as a purely or predominantly cystic lesion [12]. However, the clinical outcomes and management strategies are different between the two entities. Aggressive surgical resection is usually not optimal for LRCCs because of the higher rate of postoperative endocrine dysfunction and no reduction in recurrence rate compared to less extensive resection [3, 13, 14]. In contrast, CCPs should be followed and managed aggressively because of their high recurrence rates and relatively high rate of long-term morbidities, such as visual field defects and neurobehavioral abnormalities [15, 16, 17]. The pretreatment diagnosis of LRCCs and CCPs is important to predicting the outcome and planning the most appropriate therapeutic approach. This retrospective study was designed to evaluate the clinical and imaging findings of LRCCs and CCPs, aiming to provide clues about their pretreatment diagnosis and outcome prediction.

Methods

Patients

This study was approved by the Institutional Review Board of our hospital and followed all applicable laws, regulations, and policies for the protection of human participants.

We retrospectively reviewed brain tumors in the pathology archives and PACS of our institution from 2015 to 2021 and found 257 patients with RCCs and craniopharyngiomas. Because typical RCCs are usually not difficult to diagnose based on their locations and relatively small tumor sizes, we specifically evaluated LRCCs (measuring larger than 20 mm in diameter), which can mimic other sellar/suprasellar cystic lesions. We also collected CCPs measuring more than 20 mm in diameter for comparison. In total, 49 patients with LRCCs and CCPs met our inclusion criteria. Four patients with no DWI data were excluded (Supplemental Fig. 1).

In total, we enrolled 45 patients with pathologically proven LRCCs and CCPs, including 20 patients (8 men and 12 women) with RCCs and 25 patients (10 men and 15 women) with CCPs (Table 1). The histologic

work-up of the 25 cases of CCPs revealed an adamantinomatous subtype in 24 patients and papillary subtype in 1 patient.

Table 1
Clinical data and MR findings of the 45 patients with large Rathke's cleft cysts and cystic craniopharyngiomas.

Patient Data	Large Rathke's cleft cysts (n = 20)	Cystic Craniopharyngiomas (n = 25)	*p* Value
BASIC DATA			
Age, mean ± SD (range), y *	49.0 ± 16.8 (16–74)	34.2 ± 22.2 (1–74)	**.022**
Sex, male/female ratio	8:12	10:15	1.000
Symptoms - n (%)			
Headache - n (%)	10 (50.0)	8 (32.0)	.241
Visual impairment- n (%)	17 (85.0)	23 (92.0)	.642
Pituitary dysfunction - n (%)	12 (60.0)	15 (60.0)	1.000
Growth retardation - n (%)	0 (0)	4 (16.0)	.117
Follow-up period, mean ± SD (range), m *	25.2 ± 21.8 (3–75)	42.4 ± 24.1 (7–92)	**.010**
CLINICAL OUTCOME			
Tumor resection *			**< .001**
Gross or near-total resection - n (%)	6 (30.0)	15 (60.0)	
Subtotal resection - n (%)	2 (10.0)	10 (40.0)	
Fenestration – n (%)	12 (60.0)	0 (0.0)	
Residual tumor - n (%)	13 (65.0)	10 (40.0)	.099
Postoperative complication - n (%) *	10 (50.0)	21 (84.0)	**.006**
Diabetes insipidus - n (%) *	6 (30.0)	17 (68.0)	**.017**
Panhypopituitarism - n (%) *	3 (15.0)	12 (48.0)	**.021**
CSF leakage - n (%)	2 (10.0)	5 (20.0)	.437
Recurrence – n (%) *	2 (10.0)	10 (40.0)	**.025**
Size of recurrent tumor, mean ± SD (range), mm	21.5 ± 0.8 (21–22)	18.5 ± 6.8 (11–32)	.364
Adjuvant therapy - n (%) *	2 (10.0)	14 (56.0)	**.007**

* indicates $p < 0.05$ between two groups.

Patient Data	Large Rathke's cleft cysts (n = 20)	Cystic Craniopharyngiomas (n = 25)	*p* Value
BASIC DATA			
Repetitive surgery - n (%)	2 (10.0)	7 (28.0)	.138
Irradiation - n (%) *	1 (5.0)	11 (44.0)	**.004**
IMAGING FINDING (1): ANATOMY			
Tumor size, mean ± SD (range), mm	26.3 ± 5.8 (20–39)	29.0 ± 5.8 (21–40)	.063
Shape *			**< .001**
Lobulated appearance - n (%)	2 (10.0)	24 (96.0)	
Snowman appearance - n (%)	18 (90.0)	1 (4.0)	
Off-midline - n (%) *	0 (0)	10 (40.0)	**.001**
Growth pattern (sagittal imaging)			
Distance of mass to mesencephalon, mean ± SD (range), mm *	13.7 ± 3.4 (6.7–19.1)	7.0 ± 4.7 (0-19.9)	**< .001**
Oblique angle of the sagittal long axis of the tumor, mean ± SD (range), degree *	89.9 ± 15.6 (70–132)	107.1 ± 16.6 (76–135)	**.001**
Compression on the optic chiasm - n (%)	20 (100)	25 (100)	1.000
Optic chiasm displacement *			**< .001**
Superior - n (%)	20 (100)	8 (32.0)	
Ventral - n (%)	0 (0)	17 (68.0)	
Optic tract edema - n (%)	1 (5.0)	2 (8.0)	1.000
IMAGING FINDING (2): MORPHOLOGY			
Solid component - n (%) *	7 (35.0)	21 (84.0)	**.001**
Enhancement pattern of the cyst wall *			**.009**
No enhancement or thin (< 2 mm)	18 (90.0)	13 (52.0)	
Thick (≥ 2 mm)	2 (10.0)	12 (48.0)	
Septation - n (%) *	1 (5.0)	8 (32.0)	**.030**
Fluid–fluid level - n (%)	1 (5.0)	7 (28.0)	.059

* indicates $p < 0.05$ between two groups.

Patient Data	Large Rathke's cleft cysts (n = 20)	Cystic Craniopharyngiomas (n = 25)	*p* Value
BASIC DATA			
Hemosiderin rim - n (%)	0 (0)	1 (4.0)	1.000
Absence of the posterior pituitary bright spot - n (%)	7 (35.0)	9 (36.0)	1.000
IMAGING FINDING (3): SIGNAL INTENSITY			
Signal intensity of cystic content on T2			.118
Hyperintense - n (%)	15 (75.0)	23 (92.0)	
Iso- or hypointense - n (%)	5 (25.0)	2 (8.0)	
Signal intensity of cystic content on T1			.191
Hyperintense - n (%)	8 (40.0)	5 (20.0)	
Iso- or hypointense - n (%)	12 (60.0)	20 (80.0)	
Signal intensity of cystic content on DWI			.444
Isointense - n (%)	1 (5.0)	0 (0)	
Hypointense - n (%)	19 (95.0)	25 (100)	
ADC value, mean ± SD (range)			
White matter ($\times 10^{-3}$ mm^2/sec)	0.71 ± 0.06 (0.51–0.78)	0.76 ± 0.08 (0.64–0.99)	.147
$Cyst_{min}$ ($\times 10^{-3}$ mm^2/sec)	2.42 ± 0.53 (1.32–3.11)	2.53 ± 0.23 (1.91–2.84)	.648
$rCyst_{min}$	3.38 ± 0.66 (2.30–4.29)	3.37 ± 0.44 (2.28–4.25)	.664
$Cyst_{mean}$ ($\times 10^{-3}$ mm^2/sec)	2.52 ± 0.49 (1.42–3.16)	2.60 ± 0.22 (1.98–2.95)	.954
$rCyst_{mean}$	3.52 ± 0.59 (2.70–4.36)	3.47 ± 0.44 (2.65–4.33)	.465
Wall ($\times 10^{-3}$ mm^2/sec)	2.03 ± 0.45 (1.19–2.96)	1.96 ± 0.27 (1.42–2.52)	.545
* indicates $p < 0.05$ between two groups.			

Clinical presentation

In all patients, a careful evaluation of the clinical manifestations and neurologic examination results was performed. Preoperative and postoperative endocrinologic evaluations consisting of serum hormone concentration measurements were also performed (Table 1).

Thirty-five patients received transsphenoidal surgery, and ten received transcranial surgery. The outcomes of the surgical resections were evaluated based on the operative report and the early postprocedural MRI acquired during follow-up within 1 month. Surgical complications such as central diabetes insipidus, panhypopituitarism, or CSF leakage were assessed according to medical records. The follow-up period after the operation for these 45 patients ranged between 3 and 92 months, with a mean of 34.8 months. After the early postprocedural MRI of the sella in the first month, all patients had regular postoperative outpatient follow-up examinations every 3 months in the first year and then every 6 to 12 months. Any local recurrence and the associated adjuvant therapy provided were recorded.

MRI protocol

MR images were obtained with a 1.5 T system (Signa HDxt and Optima MR450w, General Electric Healthcare, Milwaukee, USA). The following pulse sequences focusing on the sellar and suprasellar regions were acquired: sagittal T1-weighted imaging, coronal T1-weighted imaging, axial T2-weighted imaging, coronal T2-weighted imaging, and gadolinium-enhanced axial, sagittal, and coronal T1-weighted images. Axial diffusion-weighted imaging (DWI) of the brain was perfromed using a spin—echo echo-planar sequence, with *b* values = 0, 1000 sec/mm [2]. The apparent diffusion coefficient (ADC) map was produced by the scanner software.

MRI findings

Two neuroradiologists (one with 24 years of experience and one with 4 years of experience in neuroradiology) reviewed the images retrospectively. The two readers reviewed the images independently and were blinded to the clinical information. The final results were decided in consensus by the two readers if discrepancies existed. Tumor size was calculated in centimeters using the single largest diameter on MRI scans. Cystic portions were defined as homogeneous, nonenhancing, or sharply delineated areas on MRI scans. Solid components included the enhancing portion of the tumors and the intracystic nodules (Fig. 1) [18]. Several well-known parameters of sella/suprasellar lesions were also recorded, including the normal posterior pituitary bright spot on T1WI, septation, fluid—fluid level, hemosiderin rim, and optic tract edema [19–22].

Tumor shapes were classified as a snowman or a lobulated appearance; a snowman shape was defined as a figure-eight-like shape, and a lobulated shape was defined as having two or more lobes (Fig. 2) [23]. Off-midline location was defined as lateralization of the lesion in the sella/suprasellar region on coronal images [20]. To evaluate the growth pattern of the tumor, we used two parameters evaluated on the mid-sagittal plane: distance of the mass to the mesencephalon (MM distance), and oblique angle of the sagittal long axis of the tumor (Fig. 3). The MM distance was the shortest distance between two lines parallel to the brainstem axis, between the dorsal margin of the cystic tumor and the anterior surface of the midbrain. For the oblique angle of the sagittal long axis of the tumor, we measured the angle between

two lines: the line parallel to the sagittal long axis of the tumor and the line parallel to the frontal base or the planum sphenoidale (Fig. 3). In addition, we also recorded the adjacent structures compressed by the tumors. Displacement of the optic chiasm was defined as the location relative to the tumor, either superiorly or ventrally.

The enhancement patterns of the cyst wall were classified as none, thin (enhancing wall thickness less than 2 mm), or thick (thickness equal to or more than 2 mm) (Fig. 2) [23]. Signal intensities of the cystic content of the tumors on T1-weighted, T2-weighted, and diffusion-weighted MRI scans were also evaluated. We measured the ADC value for several regions of interest (ROIs) placed in the fluid component and the wall of the lesion [24, 25]. Small ROIs of the fluid component were purposely placed over different regions in the lesion with the lowest ADC values and expressed as the minimum ADC values of the cyst. A larger ROI was chosen for the central part of the lesion, which was used to express the mean ADC value of the cyst. ROIs of the cystic wall (expressed as ADC value of the wall) were placed either over the gadolinium (Gd)-enhanced components or the outermost part abutting the cerebrospinal fluid in the interpeduncular cistern to avoid the influence of cystic, hemorrhagic, or calcified regions on volume averaging to calculate ADC values. For comparison, ADC values were measured as a control in the normal white matter of the corona radiata (Supplemental Fig. 2). Relative ADCs were obtained by dividing the ADC values of the lesions by those of normal white matter and expressing the quotient as a ratio.

Statistical analysis

Data were analyzed by using the SPSS software package (version 25.0; SPSS®, IBM®, Armonk, NY, USA). Quantitative data are expressed as the mean ± standard deviation and were analyzed by the Mann–Whitney U test. Categorical data are expressed as a percentage and were analyzed by Fisher's exact test. $p < .05$ was considered to indicate a statistically significant difference.

Results

Clinical findings

The demographic features and clinical outcomes of the LRCC and CCP groups are summarized in Table 1. The mean ages of patients with LRCC and CCP were 49.0 and 34.2 years, respectively, with a significant difference between groups ($p = .022$). The recurrence rate was significantly higher in the CCP group than in the LRCC group (40% vs. 10%, $p = .025$), and the CCP group even had a larger extent of tumor resection (60% vs. 30%, $p < .001$). Significantly more surgical complications, including diabetes insipidus and panhypopituitarism, occurred in the CCP groups than in the LRCC group (68% vs. 30%, $p = .017$; 48% vs. 15%, $p = .021$). To control the residual and/or recurrent tumors, significantly more patients in the CCP group received adjuvant therapy, including repetitive surgery and irradiation (56% vs. 10%, $p = .007$), especially irradiation (44% vs. 5%, $p = .004$). Because of their clinical symptoms, patients with CCPs had a significantly longer follow-up period (42.4 ± 24.1 months) than patients with LRCCs (25.2 ± 21.8 months). During the follow-up period, no mortality was observed in either group.

MR features

Of all MR imaging features, lobulated-shaped tumors were significantly more common in the CCP group (96%, 24 of 25 patients), and snowman-shaped tumors were mostly seen in the LRCC group (90%, 18 of 20 patients) ($p < .001$). In the LRCC group, lesions with an off-midline location were not observed (0% and 40% in LRCC and CCP, respectively, $p = .001$). In terms of tumor content, tumors associated with a solid portion were more frequent in the CCP group than in the LRCC group (84% vs. 35%, $p = .001$). Septation of the cystic portion was more commonly observed in CCPs than in LRCCs (32% vs. 5%, $p = .030$). The enhancement patterns of the cystic wall were also different between the two tumors. No enhancement or just a thin enhancement pattern of the cyst wall was most frequently observed in LRCCs (90%, 18 of 20 patients), and thick wall enhancement was observed significantly more often in CCPs (48%, 18 of 25 patients, $p = .009$).

Regarding tumor growth pattern, LRCCs showed a significantly longer mass-to-mesencephalon distance (13.7 ± 3.4 cm) than CCPs (7.0 ± 4.7 cm, $p < .001$). The oblique angle of the sagittal long axis of the tumor revealed significant vertical growth for LRCCs and superoposterior growth for CCPs (89.9° vs. 107.1°, $p = .001$). We found that the optic chiasm was displaced superiorly by the tumor in all cases of LRCCs; in contrast, the optic chiasm was significantly more commonly displaced ventrally in cases of CCPs (68%, 17 of 25 patients, $p < .001$).

There was no significant difference in ADC maps between the LRCC and CCP groups, regardless of which parameters were analyzed, including the ADC values ($Cyst_{min}$ 2.42 ± 0.53 vs. 2.53 ± 0.23×10^{-3} mm^2/sec, $Cyst_{mean}$ 2.52 ± 0.49 vs. 2.60 ± 0.22×10^{-3} mm^2/sec) and relative ADCs of the cyst ($rCyst_{min}$ 3.38 ± 0.66 vs. 3.37 ± 0.44, $rCyst_{mean}$ 3.52 ± 0.59 vs. 3.47 ± 0.44) and wall (2.03 ± 0.45 vs. 1.96 ± 0.27×10^{-3} mm^2/sec). The different MRI findings of LRCCs and CCPs are summarized in Table 1.

Discussion

Although the diagnosis of LRCCs and CCPs is usually not difficult, the present study revealed different growth patterns and indifferent DWI results that have not been described in the literature. In the imaging comparison, we found that LRCCs presented with a snowman shape, minimal or thin cystic wall enhancement, the absence of a solid component, and refined midline location significantly more often than CCPs. We also found that the tumor growth patterns had a strong potential for differentiating these two entities. LRCCs had an “upward/vertical growth pattern” with superior displacement of the optic chiasm. CCPs had a “backward pattern” with a ventrally displaced optic chiasm. To date, this is the largest series on the diagnosis of LRCC and CCP using imaging features.

Although the clinical presentations were similar between the patients in the two groups, including headache, visual field defects, and pituitary hormone deficiencies, the age distribution and prognoses were different [2, 26]. A relatively young age at diagnosis and more long-term morbidity, such as visual field defects and neurobehavioral abnormalities, in addition to a higher recurrence rate, resulted in a

significantly larger decline in quality of life in the CCP group than in the LRCC group [16, 26]. Moreover, the aggressive treatments and associated adjuvant irradiation of CCPs resulted in more frequent treatment-related complications (68% rate of diabetes insipidus and 48% rate of panhypopituitarism) [27]. In contrast, the low recurrence rate of LRCCs meant that less aggressive follow-up and treatment, such as partial cyst wall fenestration with fluid drainage, were reasonable [13, 14]. However, the extent of tumor resection should be based on the clinical presentation and the intraoperative frozen section biopsy results. Therefore, the pretreatment differential diagnosis between these two entities is important to predicting the outcome and planning the most appropriate therapeutic approach.

In addition to morphological differences, the present study showed different growth patterns between these two large cystic tumors that were not described before. An upward/vertical growth pattern for LRCCs and a backward growth pattern for CCPs were found (Fig. 1). We hypothesized that the tumor rigidity resulting from the solid and calcified components, cystic wall thicknesses and embryological origins of the two tumors may account for these tumor growth patterns. As a cystic lesion located in the pars intermedia without large solid and calcified components, RCCs may not be as stiff as CCPs. Therefore, the growth of RCCs was easily limited and directed by adjacent structures. From a coronal view, the growth limitation by the diaphragma sellae and bilateral internal carotid artery forms the “waist” of the “snowman appearance” for LRCCs (Fig. 3) [28]. RCCs tend to grow in the direction with the lowest resistance, upward along the chiasmatic cistern, and then push the optic chiasm superiorly. In contrast, the relatively thick wall and associated solid and even calcified component of CCPs may lead to a stiff consistency and exert strong resistance against adjacent structures, which results in a relatively unpredictable growth directions or even backward growth. In the coronal view, the unpredictable growth directions leads to the classic “lobulated appearance” of CCPs (Fig. 3). This stiff tumor consistency of CCPs may also explain their off-midline extension. In addition, embryonic squamous remnants of Rathke’s pouch are located along the pituitary stalk, from which craniopharyngiomas may originate [11]. The CCP tumors have relatively unlimited growth and a more solid component, resulting in a tendency to grow dorsally toward the diencephalon. In contrast, RCCs mostly originate from the pituitary gland within the confined sella turcica.

DWI and ADC maps are used to diagnose intracranial tumors and predict the histopathological grade of the tumor. It has been reported that the ADC_{min} values of craniopharyngiomas are lower than those of RCCs [29]. However, the tumors included in our study were purely or predominantly cystic, so we had to place the ROIs in the fluid component and the wall of the lesion separately. Most of the LRCC and CCP tumors presented homogeneous hypointensity on DWI of the cystic part, without a significant difference between the two entities. Both the minimum and mean ADC values were measured. For comparison, the ADC values were also normalized using a relative ADC (rADC), which was determined by dividing the ADC values of the lesions by those of normal white matter and expressing the quotient as a ratio. No significant difference between LRCCs and CCPs was found in either ADC or rADC. The mean ADC values in our study for LRCCs and CCPs were 2.52 ± 0.49 and $2.60 \pm 0.22 \times 10^{-3}$ mm^2/sec, respectively. For comparison, the mean ADC values from the study by Kunii et al [24]. for RCCs and craniopharyngiomas

were 2.12 ± 0.29 and 1.41 ± 0.34 × 10^{-3} mm^2/sec, respectively. We think the high ADC values seen in our study are attributed to both the greater freedom for water molecules to move within the fluid-rich environments of the large tumors and less influence from calcification within the predominantly cystic craniopharyngiomas, although the actual histology of the cystic component was not available in our original pathology report.

RCC and CCP cysts may show signal intensity against the cerebrospinal fluid that varies according to the cyst contents, especially the amount of protein, although the cysts are more often hypointense on T1-weight images and hyperintense on T2-weighted images [30]. In our study, the signal intensity of the cysts on T1 and T2 images did not reveal a significant difference between the two entities. We suggest that these ectodermal lesions potentially represent a continuum with the same embryonic origin, making the signal characteristics indistinguishable between RCC and CCP cysts [7, 31].

In this study, the outcomes of CCPs were much worse than those of LRCCs. In addition the different pathological characteristics of the 2 tumors, we propose the following explanations: 1) different growth patterns: the backward growth pattern of CCPs may make the lesions extend to the interpenduncular cistern and possibly abut the branches of the basilar artery and cranial nerves, making total resection of the tumor difficult. In contrast, LRCCs extend superiorly into regions without large vessels (ex. third ventricle), making complete surgical resection easy, even if total resection is not always indicated for this disease entity. In addition, the optic chiasm ventrally displaced by CCPs may sometimes limit the subfrontal surgical approach. 2) Regarding the midline suprasellar location, all the LRCCs in this study had midline locations, but 40% of the CCPs extended laterally. Lateral tumor extension can increase the degree of difficulty for total tumor removal, especially with the transsphenoid surgical approach. 3) In terms of tumor rigidity, CCPs had both solid and calcified components with thick cystic walls, which can lead to greater tumor stiffness than in LRCCs with mainly thin cystic walls. In addition to the hard tumor texture, CCPs can also present with a backward growth pattern and are more difficult to totally resect when a small surgical field is established.

There were several limitations in our study. This was a retrospective study with possible selection bias. The number of patients in this study was relatively small, which made analysis difficult. Although both cystic tumors had different clinical and imaging features in many instances, the present study provided additional clues for diagnosis when the lesions show similar presentations. We suggest further prospective studies with more patients that use high-resolution imaging techniques to enhance the diagnostic accuracy for these two entities.

Conclusions

Although the diagnosis of LRCCs and CCPs may not be difficult in some instances, this study revealed their particular growth patterns and similar DWI results that have not been described before. Pretreatment clinical and MR findings provide evidence to differentiate LRCCs from CCPs. For LRCCs, MR findings revealed a snowman appearance caused by the diaphragma sellae on coronal images, minimal or thin

cyst wall enhancement, the absence of a solid component, and a refined midline location. The different tumor rigidities and the embryological origin may also result in an upward/vertical growth pattern for LRCCs and backward growth pattern for CCPs; this may allow for an appropriate pretreatment diagnosis and help guide the selection of a surgical approach. We suggest applying these findings to improve the outcomes of sellar and suprasellar cystic tumors.

Declarations

This study has received funding from Taipei Veterans General Hospital, Taiwan [V111B-032, V112B-007 (to CHW); V110C-037, V111C-028, V112C-059, V112D67-002-MY3-1 (to FCC); V112B-005 (to STC); V112B-032 (to TML)], Veterans General Hospitals and University System of Taiwan Joint Research Program [VGHUST 109V1-5-2 and VGHUST 110-G1-5-2 (to FCC)], Ministry of Science and Technology (National Science and Technology Council) of Taiwan [MOST 110-2314-B-075-005- and 111-2314-B-075-025-MY3 (to CHW); MOST 109-2314-B-075-036 and 110-2314-B-075-032 (to FCC); MOST 110-2314-B-075-035-MY2 (to STC)], Yen Tjing Ling Medical Foundation, Taiwan [CI-109-3, CI-111-2, CI-112-2 (to CHW)], Professor Tsuen CHANG's Scholarship Program from Medical Scholarship Foundation In Memory Of Professor Albert Ly-Young Shen (to CHW) and Vivian W. Yen Neurological Foundation (to CHW and FCC).

Competing interest The authors declare no competing interests.

References

1. Potts MB, Jahangiri A, Lamborn KR, Blevins LS, Kunwar S, Aghi MK. Suprasellar Rathke cleft cysts: clinical presentation and treatment outcomes. Neurosurgery. 2011;69(5):1058-1068; discussion 1068-1067. https://doi.org/10.3389/fgene.2018.00049
2. Han SJ, Rolston JD, Jahangiri A, Aghi MK. Rathke's cleft cysts: review of natural history and surgical outcomes. J Neurooncol. 2014;117(2):197-203. https://doi.org/10.1007/s11060-013-1272-6
3. Zada G. Rathke cleft cysts: a review of clinical and surgical management. Neurosurg Focus. 2011;31(1):E1. https://doi.org/10.3171/2011.5.FOCUS1183
4. Naik VD, Thakore NR. A case of symptomatic Rathke's cyst. BMJ Case Rep. 2013;2013:bcr2012006943. https://doi.org/10.1136/bcr-2012-006943
5. Andrysiak-Mamos E, Sagan K, Sagan L, Sowinska-Przepiera E, Syrenicz A. Cystic lesions of the sellar-suprasellar region - diagnosis and treatment. Endokrynol Pol. 2018;69(2):212-228. https://doi.org/10.5603/EP.2018.0023
6. Garnett MR, Puget S, Grill J, Sainte-Rose C. Craniopharyngioma. Orphanet J Rare Dis. 2007;2:18. https://doi.org/10.1186/1750-1172-2-18
7. Harrison MJ, Morgello S, Post KD. Epithelial cystic lesions of the sellar and parasellar region: a continuum of ectodermal derivatives? J Neurosurg. 1994;80(6):1018-1025. https://doi.org/10.3171/jns.1994.80.6.1018

8. Fujio S, Hanada T, Yonenaga M, et al. Surgical aspects in craniopharyngioma treatment. Innov Surg Sci. 2021;6(1):25-33. https://doi.org/10.1515/iss-2019-1004
9. Muller HL. The diagnosis and treatment of craniopharyngioma. Neuroendocrinology. 2020;110(9-10):753-766. https://doi.org/10.1159/000504512
10. Isono M, Kamida T, Kobayashi H, Shimomura T, Matsuyama J. Clinical features of symptomatic Rathke's cleft cyst. Clin Neurol Neurosurg. 2001;103(2):96-100. https://doi.org/10.1016/s0303-8467(01)00121-4
11. Muller HL. Craniopharyngioma. Endocr Rev. 2014;35(3):513-543. https://doi.org/10.1210/er.2013-1115
12. Fahlbusch R, Honegger J, Paulus W, Huk W, Buchfelder M. Surgical treatment of craniopharyngiomas: experience with 168 patients. J Neurosurg. 1999;90(2):237-250. https://doi.org/10.3171/jns.1999.90.2.0237
13. Aho CJ, Liu C, Zelman V, Couldwell WT, Weiss MH. Surgical outcomes in 118 patients with Rathke cleft cysts. J Neurosurg. 2005;102(2):189-193. https://doi.org/10.3171/jns.2005.102.2.0189
14. Kinoshita Y, Taguchi A, Yamasaki F, Tominaga A, Arita K, Horie N. Natural course of Rathke's cleft cysts and risk factors for progression. J Neurosurg. 2022:1-7. https://doi.org/10.3171/2022.7.JNS22716
15. Turel MK, Tsermoulas G, Gonen L, et al. Management and outcome of recurrent adult craniopharyngiomas: an analysis of 42 cases with long-term follow-up. Neurosurg Focus. 2016;41(6):E11. https://doi.org/10.3171/2016.9.FOCUS16315
16. Yano S, Kudo M, Hide T, et al. Quality of life and clinical features of long-term survivors surgically treated for pediatric craniopharyngioma. World Neurosurg. 2016;85:153-162. https://doi.org/10.1016/j.wneu.2015.08.059
17. Kilic M, Can SM, Ozdemir B, Tanik C. Management of craniopharyngioma. J Craniofac Surg. 2019;30(2):e178-e183. https://doi.org/10.1097/scs.0000000000005136
18. Byun WM, Kim OL, Kim D. MR imaging findings of Rathke's cleft cysts: significance of intracystic nodules. AJNR Am J Neuroradiol. 2000;21(3):485-488.
19. Wang S, Nie Q, Wu Z, Zhang J, Wei L. MRI and pathological features of Rathke cleft cysts in the sellar region. Exp Ther Med. 2020;19(1):611-618. https://doi.org/10.3892/etm.2019.8272
20. Park M, Lee SK, Choi J, et al. Differentiation between cystic pituitary adenomas and rathke cleft cysts: a diagnostic model using MRI. AJNR Am J Neuroradiol. 2015;36(10):1866-1873. https://doi.org/10.3174/ajnr.a4387
21. Tosaka M, Sato N, Hirato J, et al. Assessment of hemorrhage in pituitary macroadenoma by T2*-weighted gradient-echo MR imaging. AJNR Am J Neuroradiol. 2007;28(10):2023-2029. https://doi.org/10.3174/ajnr.A0692
22. Kumar S, Kumar A, Gill MS, Maheshwari V. Optic tract edema: a rare entity in pituitary macroadenoma. Asian J Neurosurg. 2019;14(1):307-309. https://doi.org/10.4103/ajns.AJNS_178_18

23. Choi SH, Kwon BJ, Na DG, Kim JH, Han MH, Chang KH. Pituitary adenoma, craniopharyngioma, and Rathke cleft cyst involving both intrasellar and suprasellar regions: differentiation using MRI. Clin Radiol. 2007;62(5):453-462. https://doi.org/10.1016/j.crad.2006.12.001
24. Kunii N, Abe T, Kawamo M, Tanioka D, Izumiyama H, Moritani T. Rathke's cleft cysts: differentiation from other cystic lesions in the pituitary fossa by use of single-shot fast spin-echo diffusion-weighted MR imaging. Acta Neurochir (Wien). 2007;149(8):759-769; discussion 769. https://doi.org/10.1007/s00701-007-1234-x
25. Kinoshita Y, Yamasaki F, Tominaga A, et al. Diffusion-weighted imaging and the apparent diffusion coefficient on 3T MR imaging in the differentiation of craniopharyngiomas and germ cell tumors. Neurosurg Rev. 2016;39(2):207-213; discussion 213. https://doi.org/10.1007/s10143-015-0660-0
26. Morisako H, Goto T, Goto H, Bohoun CA, Tamrakar S, Ohata K. Aggressive surgery based on an anatomical subclassification of craniopharyngiomas. Neurosurg Focus. 2016;41(6):E10. https://doi.org/10.3171/2016.9.focus16211
27. Karavitaki N, Brufani C, Warner JT, et al. Craniopharyngiomas in children and adults: systematic analysis of 121 cases with long-term follow-up. Clin Endocrinol (Oxf). 2005;62(4):397-409. https://doi.org/10.1111/j.1365-2265.2005.02231.x
28. Meyer JR, Quint DJ, McKeever PE, Boland M, Ross DA. Giant Rathke cleft cyst. AJNR Am J Neuroradiol. 1994;15(3):533-536.
29. Mahmoud OM, Tominaga A, Amatya VJ, et al. Role of PROPELLER diffusion weighted imaging and apparent diffusion coefficient in the diagnosis of sellar and parasellar lesions. Eur J Radiol. 2010;74(3):420-427. https://doi.org/10.1016/j.ejrad.2009.03.031
30. Gadelha MR, Wildemberg LE, Lamback EB, Barbosa MA, Kasuki L, Ventura N. Approach to the patient: differential diagnosis of cystic sellar lesions. J Clin Endocrinol Metab. 2022;107(6):1751-1758. https://doi.org/10.1210/clinem/dgac033
31. Alomari AK, Kelley BJ, Damisah E, et al. Craniopharyngioma arising in a Rathke's cleft cyst: case report. J Neurosurg Pediatr. 2015;15(3):250-254. https://doi.org/10.3171/2014.11.peds14370

Figures

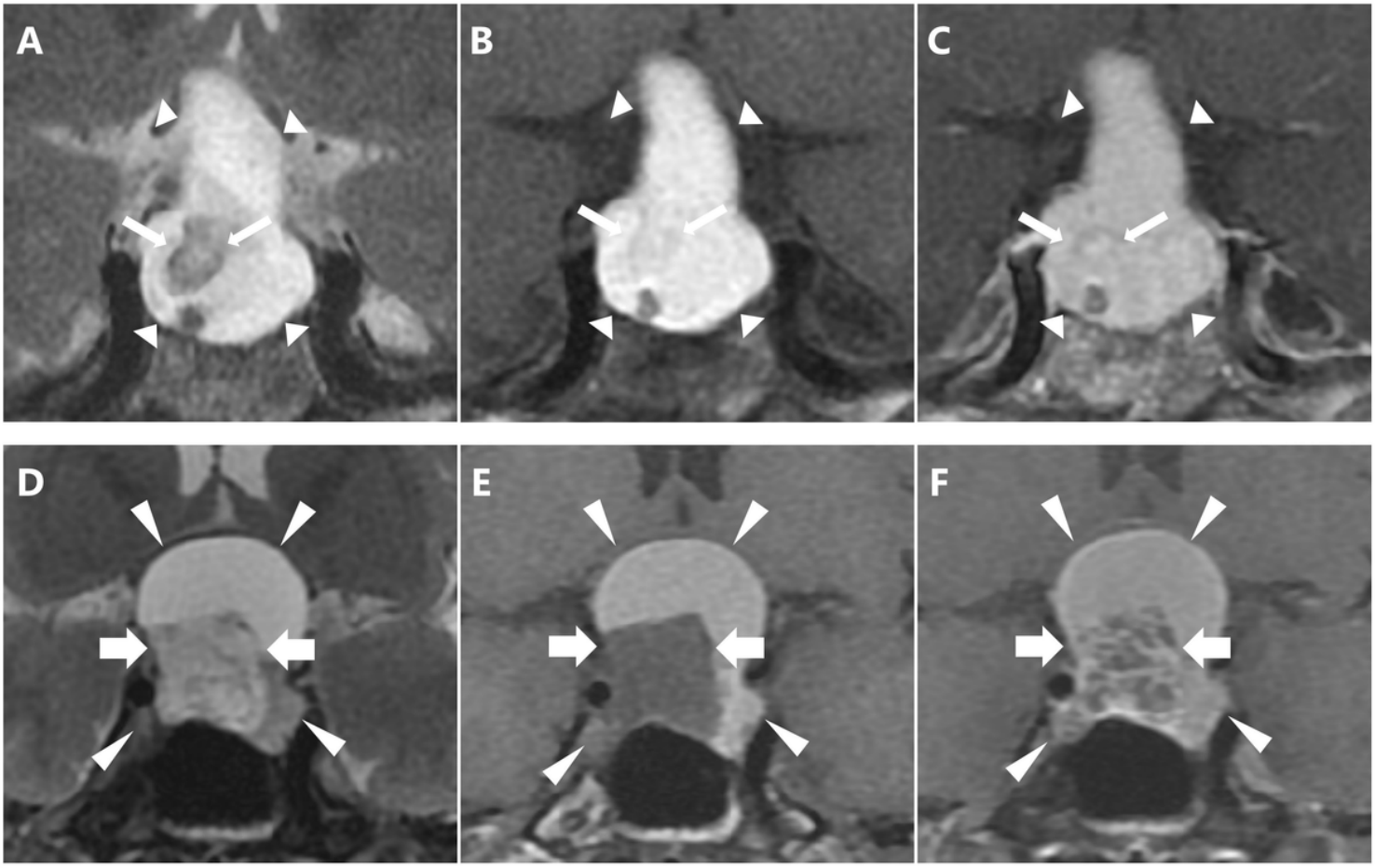

Figure 1

Example of a solid component in the cystic LRCC and CCP lesions. (A-C) A 38-year-old female patient presented with chronic headache and visual disturbance. Coronal T2WI (A), T1WI (B), and contrast-enhanced T1WI (C) sequences demonstrated a typical intracystic nodule (thin arrows) of an LRCC (short arrowheads) that appeared hypointense on T2 and isointense on T1, with no significant contrast enhancement. (D-F) Another 34-year-old female CCP patient presented with excessive thirst and peripheral visual loss. MR imaging of the solid component (thick arrows) in a CCP (long arrowheads) revealed hyperintensity on T2WI (D), hypointensity on T1WI (E), and strong enhancement on contrast-enhanced T1WI (F).

Figure 2

Example of snowman- and lobulated-shaped sellar/suprasellar cystic lesions. (A and B) A 43-year-old male patient presented with persistent headache. The coronal T2-weighted sequence demonstrated a snowman-shaped LRCC, appearing eight-like in shape with a “waist” at the level of the diaphragma sellae in the middle of the tumor (thin arrows). On sagittal contrast-enhanced T1WI (B) of the same patient, the LRCC showed thin rim enhancement of the cyst wall measuring less than 2 mm (long arrowheads). (C and D) A 14-year-old male CCP patient presented with growth retardation. A tumor with two or more lobes revealed by coronal T2-weighted images (C) and sagittal contrast-enhanced T1WI (D) was defined as lobulated in shape (thick arrows). The CCP also showed irregularly thick enhancement of the cyst wall

measuring more than 2 mm (short arrowheads) and the presence of septation within the cystic tumor (asterisk).

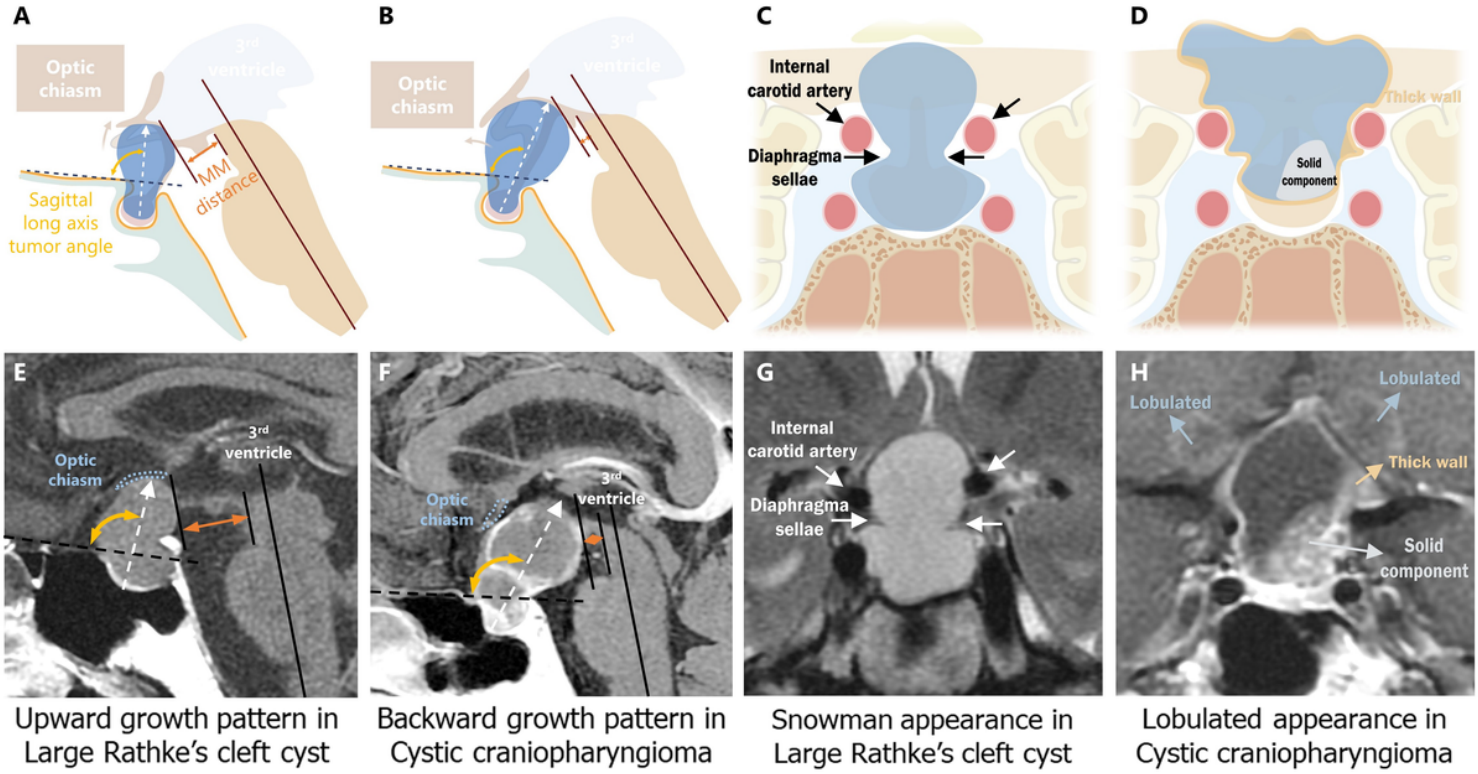

Figure 3

Evaluation of the growth patterns of LRCCs and CCPs. Lesions were subclassified into upward/vertical (A and E, LRCC) and backward (B and F, CCP) growth patterns. With an upward/vertical growth pattern (A and E), the tumor grew vertically and pushed the optic chiasm upward. With a backward growth pattern (B and F), the tumor grew along the long axis direction of the third ventricle. The optic chiasm was subsequently displaced ventrally. In the images (A and B), the methods to measure the MM distance and oblique angle of the sagittal long axis of the tumor are shown (described in the text). (C and G) Because of the less stiff consistency of LRCCs, tumor growth is limited by the surrounding diaphragma sellae and bilateral internal carotid artery, which form the "waist" of the "snowman appearance". (D and H) The thick wall and associated solid and evenly calcified component in CCPs result in its stiff character and strong resistance against adjacent structures. The directions of free growth in the CCP lead to the classic "lobulated appearance". MM distance, distance of the mass to the mesencephalon.

Supplementary Files

This is a list of supplementary files associated with this preprint. Click to download.

- SupplementalData.docx